THE JOURNAL OF PHYSICAL CHEMISTRY C

Article

pubs.acs.org/JPCC

Insights into the Charge Carrier Terahertz Mobility in Polyfluorenes from Large-Scale Atomistic Simulations and Time-Resolved Terahertz Spectroscopy

Nenad Vukmirović,*[,†] Carlito S. Ponseca, Jr.,[‡] Hynek Němec,[§] Arkady Yartsev,[‡] and Villy Sundström[‡]

[†]Scientific Computing Laboratory, Institute of Physics Belgrade, University of Belgrade, Pregrevica 118, 11080 Belgrade, Serbia

[‡]Division of Chemical Physics, Lund University, Box 124, 221 00 Lund, Sweden

[§]Institute of Physics, Academy of Sciences of the Czech Republic, 182 21 Prague, Czech Republic

Supporting Information

ABSTRACT: Multiscale atomistic simulations were used to understand the factors that determine the charge carrier mobility spectrum obtained from time-resolved terahertz (THz) spectroscopy in conjugated polymers. The simulation approach combines classical molecular dynamics simulations of atomic structure, large-scale electronic structure calculations, and the evaluation of the THz mobility using Kubo's linear response formula. We found that THz radiation probes a single carrier hop at low temperatures and high frequencies, while the transport over somewhat longer distances is probed in the opposite cases. Our results indicate that charge carrier transport at THz frequencies is thermally activated but with a much smaller activation energy compared to the dc case. The shape of the real and imaginary part of the mobility spectral curve reveals the presence of above THz hopping rates that are relevant for charge carrier transport. Strong differences of the mobilities in the polymer and the corresponding monomer material are largely caused by stronger energetic disorder of the monomer material.

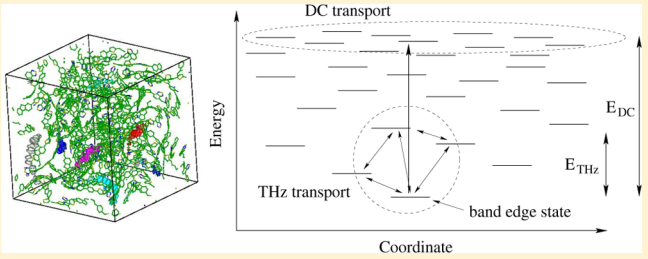

INTRODUCTION

Charge carrier transport in organic semiconducting polymers is a topic of high current interest for the development of organic electronic and optoelectronic components.[1−8] Several experimental techniques are currently available to probe the dc transport in these materials. The dc mobility can be extracted from field-effect transistor characteristics, the diode characteristics in space−charge limited current regime, or the time-of-flight technique.[8,9] The dc mobility gives the information about the ability of charge to travel over long distances. Organic polymers typically exhibit a large degree of disorder that originates from the irregular shape of the polymer chains. This translates into a significant number of trap states from which a carrier can escape by thermal excitation only. Consequently, the dc transport is thermally activated with activation energies which can be as large as 350 meV in the case of the poly(3-hexylthiophene) (P3HT) polymer as obtained both in experiments[10,11] and multiscale atomistic simulations.[12]

On the other hand, in many regimes of interest in typical devices, the dc mobility is not the quantity of most significant interest. For example, in bulk heterojunction-based solar cells,[13] photogenerated carriers travel within very short distances over very short times before they reach the interface between the two materials. To probe charge carrier motion over short time and length scales, the probes that access these scales are necessary. In the past decade, time-resolved THz spectroscopy[14,15] was established as a powerful technique for probing the charge carrier dynamics at picosecond time scales. It provides the understanding of fundamental microscopic processes that take place in a given material by noncontact probing of the response of charge carriers to THz electromagnetic radiation. Within this technique one is capable of extracting the charge carrier conductivity and mobility spectrum from the measured transmittance spectrum.[14,15]

The spectrum of frequency-dependent mobility encodes in principle the information about the charge carrier hopping rates and distances and the nature of charge carrier transport. However, it is not an easy task to extract this wealth of information from a single spectral curve. Therefore, a detailed understanding of the relation between the microscopic charge carrier hopping processes and THz mobility is certainly sought for.

In this work, we shed light on this relation using multiscale simulations that link the atomic structure of the material and the THz mobility spectra. We gain insight into this relation by several means: (a) In microscopic simulations we decompose the mobility into contributions from carriers that travel along various distances with various energies and identify the dominant contributions. (b) We establish the relation between the shape of the spectrum and the carrier hopping rates. (c) We

Received: June 5, 2012
Revised: July 31, 2012
Published: August 22, 2012

   dx.doi.org/10.1021/jp3055262 | J. Phys. Chem. C 2012, 116, 19665−19672

compare the mobility spectra of a polymer to its monomer with and without alkyl side chains and consequently gain insight into the role of chemical structure of the material. (d) We compare the simulated mobility spectra to experimental data obtained using time-resolved THz spectroscopy and gain insights that can be obtained by merging the conclusions from theory and experiment.

As a material for this case study, we have chosen a polyfluorene copolymer poly[2,7-(9,9-dioctyl-fluorene)-*alt*-5,5-(4′,7′-di-2-thienyl-2′,1′,3-benzo-thiadiazole)] (APFO-3). The structural formula of this polymer is shown in Figure 1. One

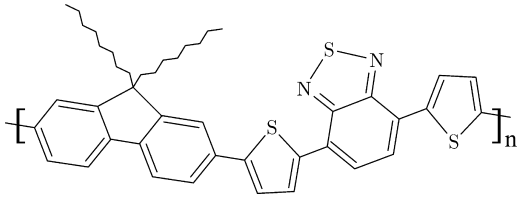

Figure 1. Chemical formula of APFO-3 polymer.

period of the polymer consists of a fluorene unit and the benzothiadiazole acceptor unit sandwiched between the two thiophene donor units. This material and its applicability for organic photovoltaics have been studied in the past.[16−19] The presence of a donor−acceptor−donor part in the copolymer leads to a relatively low band gap of the polymer which translates into the ability to absorb a large part of the solar spectrum. On the other hand, the fluorene unit enables good electrical transport characteristics typical for polyfluorenes.[18] Promising characteristics of solar cells based on this material have been reported.[17] Recent time-resolved THz spectroscopy studies[20,21] of the APFO-3 material blended with fullerenes have provided a wealth of experimental data that can be compared with simulations presented here and further interpreted with the aid of simulation results.

SIMULATION METHODOLOGY

In this section, we describe the simulation methodology that we used to link the atomic structure of the material to its mobility at THz frequencies. The general simulation strategy, schematically illustrated in Figure 2, consists of several steps. At first, we

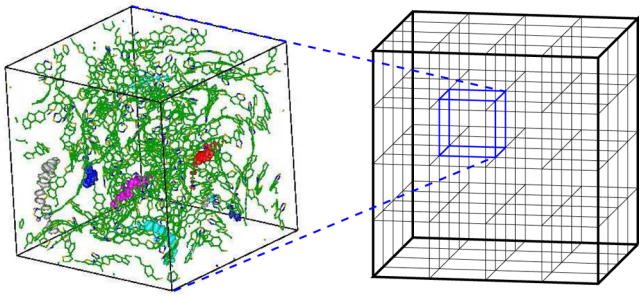

Figure 2. Scheme of the multiscale simulation procedure. Left: the probability density isosurfaces of several top states in the valence band for the 11 304 atom portion of the material. The isosurfaces correspond to 50% probability of finding the charge inside the surface. The HOMO level is shown in blue, HOMO − 1 in red, HOMO − 2 in pink, HOMO − 3 in light blue, and HOMO − 4 in gray. The corresponding eigenenergies (in eV) are, respectively, 7.303, 7.227, 7.140, 7.102, 7.096. Right: the 4 × 4 × 4 system used for the calculation of mobility.

construct the atomic structure of the material of the size ∼5 nm ×5 nm ×5 nm (left panel in Figure 2) from classical molecular dynamics (MD) simulations using a simulated annealing procedure. For this part of the material, we then calculate the energies and the corresponding wave functions of hole states and the probabilities for the hole to hop between different states. However, to get reliable information about the carrier mobility in the material, a larger simulation cell is necessary. Therefore, we repeat the previous calculation many (∼50) times and construct a larger ∼20 nm ×20 nm ×20 nm system (right panel in Figure 2). On the basis of the calculated hopping probabilities, we finally calculate the hole mobility using Kubo's linear response formula. The details of this general strategy are outlined below.

Although the approach in which classical MD simulations are combined with quantum mechanical electronic structure calculations has been used in several studies,[22−30] its extensions to the simulation of dc mobility are rather scarce,[12,31,32] and it has not yet been extended to the treatment of ac mobility.

Simulation of the Atomic Structure of the Material. Atomic structure of the material was obtained from classical MD using a simulated annealing procedure, in a similar manner as was done previously for polythiophene[28,33] and poly(aryl-ethynylene)[34] polymers. In the MD simulation, we have considered a system of 11 304 atoms (the system consists of 12 chains, each 10 monomer units long, with octyl side chains attached). Initially, the system is placed in a large box (side length of 20 nm) at a high temperature (1000 K). The box dimensions are then first gradually decreased down to 5.14 nm (which corresponds to the experimental[35] density of the material of 1 g/cm^3). Finally, the system is cooled to room temperature and relaxed to a local minimum.

In the MD simulations, we have used the CFF91 force field,[36,37] whose parameters were modified as follows. Bond lengths and angles were changed to reproduce the ones obtained from quantum chemical calculations [based on density functional theory (DFT) with the hybrid B3LYP functional[38,39] and the 6-31G basis set] of the monomer. Atomic charges in the force field were taken as the charges of the motifs used in the charge patching method (this method will be described below). A deficiency of many general classical force fields (including the CFF91) is their inability to properly describe the interring torsion potentials. Therefore, we have modified the interring torsion potential terms to reproduce the ones obtained from quantum chemical calculations. The details of the modification of the force field and the validation of the modified force field are given in the Supporting Information. MD simulations were performed using the LAMMPS code,[40,41] while the B3LYP calculation was performed using the NWChem[42] code.

Calculation of the Electronic Structure of the Material. The atomic structure obtained using the procedure outlined in the previous section was then used as input for the calculation of electronic structure of the material. Electronic structure of the material was obtained using the charge patching method (CPM)[28,43] and the overlapping fragments method (OFM).[33,44]

The CPM is a method for obtaining the electronic charge density of the system which has the accuracy similar to that of DFT in the local density approximation (LDA). It is based on the idea that the electronic charge density around an atom depends only on its local environment and that it is the same in some small prototype system and in the large system that we

dx.doi.org/10.1021/jp3055262 | J. Phys. Chem. C 2012, 116, 19665−19672

are interested in. The electronic charge density of the large system is therefore obtained by simply adding the contributions of individual atoms (these contributions are called motifs). The motifs were extracted from DFT/LDA calculations for a monomer. Once the electronic charge density is obtained, one can also get the single-particle potential experienced by an electron in the system.

Since CPM is an approximation to a full DFT/LDA calculation, it is desirable to verify its accuracy on some smaller system where it is still feasible to perform a DFT/LDA calculation. The test that verifies the accuracy of the CPM is given in the Supporting Information.

The OFM is the method for the diagonalization of a single-particle Hamiltonian, for example, the one obtained using the CPM. It is based on the division of the system into (mutually overlapping) fragments and the representation of the Hamiltonian in the basis of eigenfunctions of these fragments. The details of the application of the OFM method to the APFO-3 polymer system and the verification of its accuracy are given in the Supporting Information.

The wave functions and eigenenergies of several top states in the valence band for one realization of the 11 304 atom system are given in Figure 2, left panel. The wave functions are localized due to a disordered shape of the chains, and the charge carrier transport in the system takes place by carrier hopping between such localized states.

Calculation of Hopping Probabilities between Hole States. The probability for downhill hopping between states i and j in a unit of time should in principle be calculated by taking into account the interaction with all phonon modes as[12,45]

$$W_{ij} = \pi \sum_{\alpha} \frac{|\mathcal{M}_{ij,\alpha}|^2}{\omega_\alpha}[N(\hbar\omega_\alpha) + 1]\delta(\varepsilon_i - \varepsilon_j - \hbar\omega_\alpha) \quad (1)$$

where $\mathcal{M}_{ij,\alpha} = \langle\psi_i|\partial H/\partial\nu_\alpha|\psi_j\rangle$ is the electron−phonon coupling constant between electronic states i and j due to phonon mode α, $\partial H/\partial\nu_\alpha$ is the change of the single-particle Hamiltonian due to atomic displacements according to phonon mode α, $\hbar\omega_\alpha$ is the energy of that mode, $N(h\omega_\alpha) = (\exp(h\omega_\alpha/k_BT) - 1)^{-1}$ is the phonon occupation number given by the Bose−Einstein distribution at a temperature T, and ε_i is the energy of electronic state i.

However, such calculations for the 11 304 atom system would be too computationally demanding, because they require the calculation of the change of the single-particle Hamiltonian with respect to displacement of each atom in the system. Fortunately, we have recently shown in the case of P3HT polymer that the expression given by eq 1 can be reasonably well approximated with the expression

$$W_{ij}^{\text{model}} = \beta^2 \mathcal{S}_{ij}^{\,2}[N(\varepsilon_{ij}) + 1]D_{\text{ph}}(\varepsilon_{ij})/\varepsilon_{ij} \quad (2)$$

which assumes that $\mathcal{M}_{ij,\alpha}$ is simply proportional to the overlap $\mathcal{S}_{ij} = \int d^3\mathbf{r}|\psi_i(\mathbf{r})|\cdot|\psi_j(\mathbf{r})|$ of the wave function moduli. In eq 2, $D_{\text{ph}}(E)$ is the phonon density of states normalized such that $\int_0^\infty D_{\text{ph}}(E)\, dE = 1$, $\varepsilon_{ij} = |\varepsilon_i - \varepsilon_j|$, and β is the proportionality factor.

We find that the same expression can be used in the case of the APFO-3 polymer as well. The density of phonon states was calculated from the same classical force field used in MD simulations and is shown in Figure 7 in the Supporting Information. To extract the factor β for APFO-3, we have performed the calculation of W_{ij} (eq 1) using the methodology of ref 12 for the 2360 atom system where it is still feasible to do the calculation of all electron−phonon coupling constants. We find that the best agreement between W_{ij} and W_{ij}^{model} is achieved with the parameter $\beta = 3.7 \times 10^6$ eV s$^{-1/2}$. The comparison of W_{ij} and W_{ij}^{model} for this value of β is given in Figure 8 in the Supporting Information. A discussion of the validity of the approximation where W_{ij} is replaced by W_{ij}^{model} is also given in the Supporting Information.

With hopping rates between different states at hand, one can derive the formula for the ac mobility in the system. However, our electronic structure calculations were performed for a box of ∼5 nm size and the simulated charge motion would be artificially restricted to the box size. Despite the fact that THz radiation probes the carrier motion over short distances, we find that these distances need to be larger than ∼5 nm. This suggests that we need to go one length scale further in our simulation and construct a larger, say 4 × 4 × 4, system. The calculations for the ∼5 nm boxes were therefore repeated 50 times, and each of the cells in the 4 × 4 × 4 system corresponds to one ∼5 nm box, randomly chosen and randomly oriented. The intracell hopping rates in the 4 × 4 × 4 system are available from the calculation in the ∼5 nm box, while the intercell hopping rates were approximated in the same manner as in ref 12.

Derivation of the Formula for ac Mobility in a Hopping Model. With hopping rates between different states at hand, one can evaluate the ac mobility for carrier hopping transport as follows.

The system consists of a set of sites i with spatial coordinates $\boldsymbol{R}_i$ and energies E_i. With the probability that the carrier hops from site i to site j in a unit of time given as W_{ij}, rate equations for evolution of populations of states n_i in time are

$$\frac{dn_i}{dt} = \sum_j A_{ij} n_j \quad (3)$$

where

$$A_{ij} = W_{ji} - \delta_{ij} \sum_k W_{ik} \quad (4)$$

The carrier that is initially (at $t = 0$) placed at a certain site will hop to other sites as time evolves. Let $\Delta^2(t)$ be the mean square spread of the position of the carrier at time t. The ac mobility of the carrier is related to $\Delta^2(t)$ by Kubo's formula[15,46,47]

$$\mu(\omega) = -\frac{e\omega^2}{2k_BT}\lim_{\alpha\to 0}\int_0^\infty dt\; e^{-\alpha t}e^{i\omega t}\langle\Delta^2(t)\rangle \quad (5)$$

which is valid for carriers in thermal equilibrium at a temperature T. The factor $e^{-\alpha t}$ can be interpreted as a weak coupling of the system and the rest of universe.[46] This factor ensures the convergence of the integral in eq 5. For a carrier initially placed at site a, the mean square spread of its position at time t is given as

$$\langle\Delta^2(t)\rangle_a = \sum_i n_i^a(t)(\boldsymbol{R_i} - \boldsymbol{R_a})^2 \quad (6)$$

where $n_i^a(t)$ is the solution of the system of equations (eq 3) with the initial condition $n_i(0) = \delta_{ia}$. To calculate $\langle\Delta^2(t)\rangle$ from eq 5 one has to average $\langle\Delta^2(t)\rangle_a$ (eq 6) over all possible initial states as

dx.doi.org/10.1021/jp3055262 | J. Phys. Chem. C 2012, 116, 19665−19672

$$\langle \Delta^2(t) \rangle = \sum_a w_a \langle \Delta^2(t) \rangle_a \tag{7}$$

where

$$w_a = \frac{\exp(-E_a/k_B T)}{\sum_i \exp(-E_i/k_B T)} \tag{8}$$

One therefore obtains the following expression for the mobility

$$\mu(\omega) = -\frac{e\omega^2}{2k_B T} \sum_{i,a} w_a (\boldsymbol{R_i} - \boldsymbol{R_a})^2 \lim_{\alpha \to 0} \int_0^\infty dt\ e^{-\alpha t} e^{i\omega t} n_i^a(t) \tag{9}$$

If we denote the last integral of the above expression as

$$I_{ia} = \lim_{\alpha \to 0} \int_0^\infty dt\ e^{-\alpha t} e^{i\omega t} n_i^a(t) \tag{10}$$

and perform the integration by parts, we obtain

$$I_{ia} = \frac{n_i^a(0)}{i\omega} + \frac{1}{i\omega} \sum_j A_{ij} I_{ja} \tag{11}$$

Since $n_i^a(0) = \delta_{ia}$, the last equation in matrix form reads

$$[\mathbf{I}] = \frac{1}{i\omega} + \frac{1}{i\omega} [\mathbf{A}][\mathbf{I}] \tag{12}$$

and therefore

$$[\mathbf{I}] = (i\omega - [\mathbf{A}])^{-1} \tag{13}$$

The final expression for the mobility therefore reads

$$\mu(\omega) = -\frac{e\omega^2}{2k_B T} \sum_{i,a} w_a (\boldsymbol{R_i} - \boldsymbol{R_a})^2 [(i\omega - [\mathbf{A}])^{-1}]_{ia} \tag{14}$$

RESULTS AND DISCUSSION

Mobility of Holes in APFO-3. The ac mobility of holes in APFO-3 was calculated by modeling the transition rates between the states using eq 2 and calculating the mobility from eq 14. The calculations were repeated for 100 different realizations of the 4 × 4 × 4 system, and the final mobility is taken as the average over these realizations. The real part of the mobility for 100 different realizations of the 4 × 4 × 4 system is shown in Figure 9 in the Supporting Information. These results indicate that fluctuations of the mobility for different realizations of the system are not large and that the average of these values can be reliably taken as the mobility of the bulk material.

The frequency dependence of the mobility for several different temperatures is shown in Figure 3. We find that the real part of the mobility is positive and increases when the frequency increases, while the imaginary part of the mobility is negative and decreases (becomes more negative) when the frequency increases. Experimental time-resolved THz spectra measured by our group showed similar shape of spectra for both real and imaginary part of the mobility.[20,21] In the literature, this type of response is typically assigned to carriers that are localized.[14,15] Such a behavior differs from the Drude response of delocalized carriers, which exhibits a real part decreasing with frequency and positive imaginary part of mobility. Below we discuss the nature of the "localized" response and we draw additional conclusions on the relation between carrier transport and shape of the mobility spectrum.

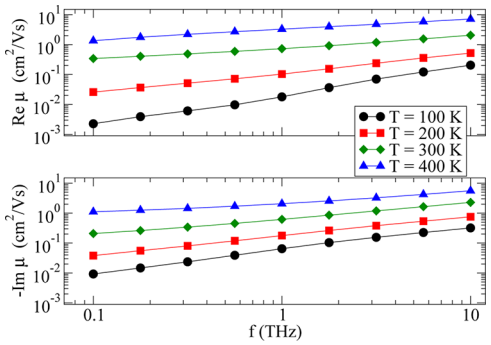

Figure 3. Frequency dependence of the mobility of holes in APFO-3 polymer at several temperatures.

First of all, the shape of the spectrum in the THz range shows that there are hopping rates well above THz frequencies that are highly relevant for the transport in the system. This was suggested in conjunction with a very simple model considering an exponential distribution of hopping times over a constant distance.[48] Here we investigate a more sophisticated toy model including a Gaussian distribution of energy levels and, namely, the relation between the distribution of hopping rates and the mobility spectrum. In such a simple model one can easily change the form of the hopping rates and consequently understand their effect on the mobility spectrum. In Figure 4,

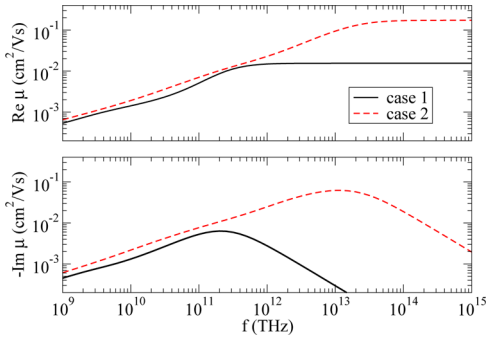

Figure 4. Charge carrier mobility in a simple one-dimensional hopping model. The lattice spacing is a = 1 nm, the temperature is T = 300 K. Site energies are assumed to have a Gaussian distribution with standard deviation σ = 0.1 eV. Downhill hopping rates are assumed to be of the form $W_{ij} = W_0 \exp(-\alpha r_{ij}/a)$, with α = 4.5, where $W_0 = 10^{14}$ s^{-1} (case 1) or $W_0 = 10^r$ s^{-1} (case 2), where r is a random number uniformly distributed between 12 and 16.

we first show the mobility spectrum when downhill hopping rates take the Miller–Abrahams form $W_{ij} = W_0 \exp(-\alpha r_{ij}/a)$, with α = 4.5, where $W_0 = 10^{14}$ s^{-1}. In this case (labeled as case 1), the largest hopping rates are between nearest neighbors and are approximately $W_{ij} = 10^{12}$ s^{-1}. In case 2 shown in Figure 4, W_0 is assumed to take the form $W_0 = 10^r$ s^{-1}, where r is a random number uniformly distributed between 12 and 16. Case 1 represents the case where there is no large dispersion in the values of hopping rates, while in case 2 the hopping rates vary by at least 4 orders of magnitude. In both cases, we find that there is a characteristic frequency $\sim \max W_{ij}/(2\pi)$. At this frequency, there is a negative peak in the imaginary part while the real part saturates above this frequency. These results therefore suggest that the mobility spectrum encodes the information about the maximal relevant hopping rates in the system. Consequently, the increasing real part and the negative

dx.doi.org/10.1021/jp3055262 | J. Phys. Chem. C 2012, 116, 19665–19672

(almost linearly decreasing) imaginary part in the APFO-3 material at THz frequencies clearly indicate that there are above-THz hopping rates that strongly contribute to the carrier mobility spectrum. We note that we have used this toy model only to understand the relation between hopping rates and the mobility spectrum. In the rest of the paper, we will present the results obtained from a detailed atomistic multiscale simulation methodology.

Deeper understanding of the type of carrier motion that leads to the measured mobility spectra is certainly sought for. Hand-waving arguments suggest that THz radiation probes the motion of carriers over short distances because the carrier does not have enough time to cross large distances during one period of the wave. However, there is a need to quantify the length of these short distances. To achieve this, we decompose eq 14 into contributions from individual terms. We then classify these terms according to the travel distance $|\boldsymbol{R}_i - \boldsymbol{R}_a|$ of the carrier. In that way, we get the distance-resolved mobility, which we show in Figure 5. At low temperatures, the carriers

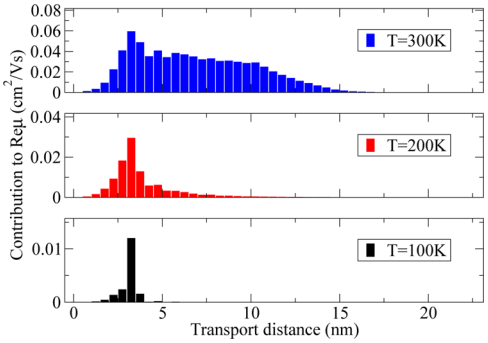

Figure 5. Distance-resolved mobility of holes in APFO-3 polymer at several temperatures and f = 1 THz.

probed by 1 THz radiation travel to the distances of the order of ∼3 nm only, which corresponds to one or two hops only. On the other hand, as the temperature increases, the probed carriers travel over larger distances. When the change of distance-resolved mobility with frequency is concerned, one can see from Figure 6 that higher frequencies probe the motion of the carriers over shorter distances, leading eventually to the probing of a single hop at a frequency which is high enough. Figure 6 indicates that at frequencies above ∼1 THz the largest contribution comes from travel distances of the order of ∼3 nm regardless of the frequency of probing radiation. This suggests that at these frequencies one has entered the regime where the

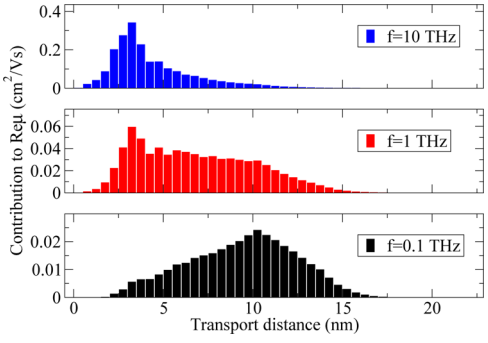

Figure 6. Distance-resolved mobility of holes in APFO-3 polymer at several frequencies and T = 300 K.

ac mobility is dominated by a single carrier hop. Consequently, the maximum of distance-resolved mobility will stay at the same position with further increase in frequency. On the other hand, at frequencies below 0.1 THz one expects that the maximum of distance-resolved mobility will shift to larger distances. However, to perform simulations at these frequencies, one needs a larger supercell and the simulations become computationally too expensive. Overall, the simulation results indicate that at low temperatures and high frequencies the THz mobility essentially represents the dynamics of hopping rates. On the other hand, at high temperatures and low frequencies, it is the transport over ∼(5−10) nm distances that gives the dominant contribution to the mobility spectrum. Transient absorption measurements previously reported by our group showed that the electron−hole separation distance right after photoexcitation is 3.4 nm for APFO-3:[60]PCBM and 4.6 nm for APFO-3:[70]PCBM.[19] This estimate can be interpreted as the distance traveled by a hole within the polymer chain where electrons in PCBM are less mobile than holes in the polymer.[21] The fact that transport distances probed by THz radiation are similar to travel distances in the process of charge generation makes time-resolved THz spectroscopy an excellent tool to investigate the process of charge generation in organic photovoltaics.

To further understand the calculated mobility spectra, and in particular its temperature dependence, we also define the energy-resolved mobility by classifying the terms in eq 14 according to the energy of the initial state E_a. This decomposition of the mobility is shown in Figure 7. The

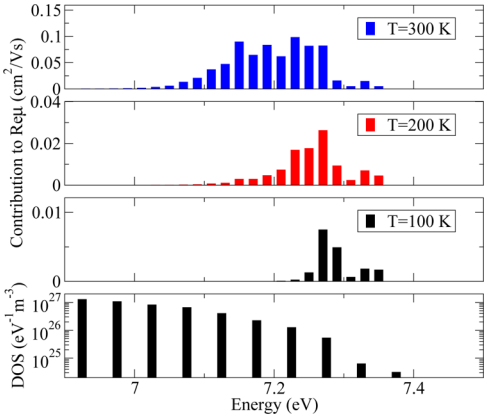

Figure 7. Energy-resolved mobility of holes in APFO-3 polymer at several temperatures and f = 1 THz. The electronic density of states is also given as the reference.

results indicate that, as the temperature increases, the contributions from energies deeper below the top of the valence band states become increasingly important. This, in turn, leads to the increase of mobility at higher temperatures as can be seen from Figure 3. Nevertheless, this increase is much smaller than for dc mobility. To quantify this difference we have performed also the simulation of dc mobility of the APFO-3 polymer using similar multiscale methodology for dc transport introduced in ref 12. We find that a rise in temperature from 200 to 400 K leads to an increase of THz mobility by a factor of 30, while at the same time the dc mobility increases by a factor of 1300.

On the basis of the results of the simulations, we can provide the following simplified picture (Figure 8) that can be used to

dx.doi.org/10.1021/jp3055262 | J. Phys. Chem. C 2012, 116, 19665−19672

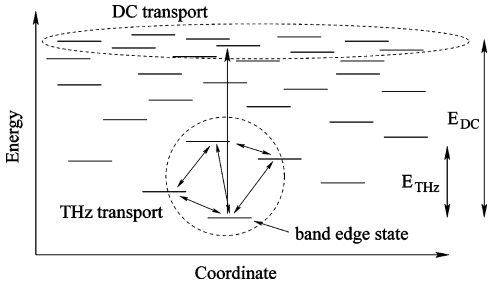

Figure 8. Schematic description of THz and dc transport in a disordered system. E_{THz} and E_{dc} correspond to rough estimates of activation energies for THz and dc transport. The energy scale is reversed in comparison to Figure 7.

understand the results obtained. The figure represents the distribution of carriers in space (x-axis) and energy (y-axis) which is typical for a disordered material. At low temperatures almost all carriers are in the ground state and can possibly hop only to some of the very few neighboring states. As a consequence, the mobility spectrum essentially describes the dynamics of single carrier hops. On the other hand, at somewhat larger temperatures the carriers start to occupy higher energy states. These are more abundant, and therefore, the carriers at these energies are capable of traveling over distances that correspond to more than a single carrier hop. The scheme from the figure also demonstrates the reason of much smaller activation energy for THz mobility in comparison to dc mobility. For THz mobility, it is sufficient to have the carriers excited to energies where a relatively large number of neighboring states exist. On the other hand to get significant values of dc mobility one must excite the carriers to a band of delocalized states, or at least to the energies where the localized states are dense enough so that a percolating path can be formed. This simplified picture can be also used to understand the frequency dependence of mobility obtained in Figure 3, where the magnitudes of both the real and imaginary parts of mobility are an increasing function of frequency. When probed by high-frequency radiation, the carriers can travel only over very short distances during the period of the wave. Therefore, the probability that the carriers will be trapped at some states from the tail of the density of states is rather low and consequently their high-frequency mobility is high. This is no longer the case when carriers are probed by low-frequency radiation: in this case, they travel over longer distances, and therefore they get frequently trapped in tail states during the period of the wave, which makes their low-frequency mobility low.

The simulations presented are based on Kubo's linear response formula which assumes that charge carriers have reached thermal equilibrium at the time of probing. In this paragraph we discuss the range of validity of such an assumption, which clearly depends on the experimental conditions. If the pump−probe delay is longer than the carrier equilibration time then the carriers are in equilibrium at the time of probing. Several studies in the past[49,50] demonstrated that the equilibration time of charge carriers strongly depends on the degree of disorder and temperature, where strong disorder and small temperatures favor large equilibration times. Our recent time-resolved THz spectroscopy studies[51] of polymer−fullerene blends at room temperature indicate that at higher photon flux the transient THz conductivity exhibits a fast (several picoseconds) decay, followed by a slower decay (hundreds of picoseconds to nanoseconds). At lower photon flux the fast decay disappears, but the slow decay remains present. The fast decay was assigned to originate from charge pair annihilation process present at high excitation densities, while it remains unclear whether the slower decay originates from charge carrier cooling or trapping. These results suggest that a certain type of quasi-equilibrium is formed several picoseconds after the excitation and that the assumption of thermal equilibrium is likely to be valid then.

Comparison of Mobilities in the Material Consisting of Polymers and Monomers. To understand the differences between the mobility of APFO-3 polymer material and the APFO-3 monomer material, we have performed detailed simulations for both of these. In contrast to APFO-3 polymers in our samples, that have octyl side chains attached to the main polymer chain, the monomers in our samples do not have the side chains. As a consequence, two effects lead to differences in the measured mobilities of the two samples: polymer versus monomer effect and the side chain effect. Concerning the polymer versus monomer effect, it is expected that the sample with polymers will exhibit a higher mobility—carriers are free to move along long polymer chains—whereas such a transport is inhibited in monomers. However, it is not straightforward to predict whether octyl side chains act to reduce or increase the mobility. On the one hand, octyl side chains act as insulating barriers, and as a consequence one may expect that they inhibit the transport since they prevent the interchain carrier hopping. On the other hand, the presence of octyl side chains also increases the distance between the main polymer chains. This acts to reduce the disorder introduced by other main polymer chains on a particular chain. Reduced disorder leads to an increase of carrier mobility.

To distinguish between the effect of side chains and the polymer versus monomer effect we have also performed the simulation on a system that consists of APFO-3 monomers with side chains. In Figure 9, we compare the mobilities of the

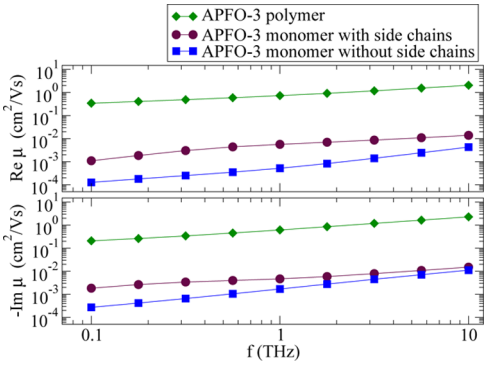

Figure 9. Frequency dependence of the mobility at T = 300 K for the material consisting of APFO-3 polymers, APFO-3 monomers with octyl side chains, and APFO-3 monomers without alkyl side chains.

three systems that we studied. APFO-3 polymer with side chains exhibits a higher mobility than APFO-3 monomer with side chains, which clearly demonstrates the role of polymer versus monomer effect. The comparison of mobilities of monomer with and without side chains indicates that the presence of side chains increases the mobility—in other words their role in reducing the disorder is more pronounced than their action as insulating barriers.

dx.doi.org/10.1021/jp3055262 | J. Phys. Chem. C 2012, 116, 19665−19672

To verify this conclusion about the importance of disorder, in Figure 10 we compare the density of electronic states of the

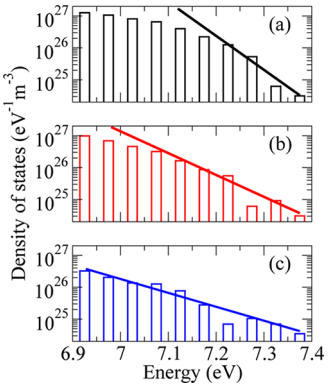

Figure 10. Comparison of the density of hole states of the material consisting of (a) APFO-3 polymers, (b) APFO-3 monomers with octyl side chains, and (c) APFO-3 monomers without alkyl side chains. The lines serve as a guide to the eye to demonstrate different widths of the tail of the density of states.

three systems studied. We find that the tail of the density of states in the monomer material with side chains is narrower than in the case of monomer without side chains, which suggests that the disorder is stronger in the material with monomers without side chains, in agreement with the previous conclusion. The strength of the disorder originates from the presence of built-in electric dipoles in the donor−acceptor part of the system. In a disordered system, these dipoles are randomly oriented and each of them creates an electrostatic field which causes the fluctuations in the single-particle potential through space.

Results of THz time-resolved experiments on the APFO-3 monomer without side chains and the APFO-3 polymer, both blended with PCBM, showed 6 times difference in their transient photoconductivity. We were able to show that, for APFO-3 monomer blend, the THz radiation probes the motion of electrons in PCBM, while for APFO-3 polymer blend it is the mobility of holes in the polymer that is probed.[21] This is consistent with the calculation where the hole mobility for the monomer is 3 orders of magnitude less than the hole mobility in the polymer. Furthermore, by increasing the number of repeat units in the polymer from 26 to 150, we obtained a systematic increase in the hole THz mobility.[21] This is also in agreement with the calculation results where less disorder (longer polymer chain) is associated with higher hole mobility.[21]

CONCLUSIONS

In conclusion, we have used atomistic multiscale simulations to understand the origin of the carrier mobility spectrum in disordered organic polymers at THz frequencies and the information that can be extracted from such experimental spectra. We find that at high frequencies and low temperatures the THz radiation probes essentially a single carrier hop, while otherwise it probes the carrier transport over somewhat longer (∼5−10 nm) distances. This leads to a temperature dependence with much smaller activation energy in comparison to dc transport. The shape of the real and imaginary part of the mobility spectrum suggests that hopping rates at frequencies higher than THz are also of high relevance for the transport in the system. Comparison of the mobilities of monomer and polymer material indicates that better transport in polymer material originates not only from the ability of the carrier to travel over longer distances in polymer material but also from the higher energetic disorder in the monomer material. Our results decipher the information encoded in the THz mobility spectrum, contribute to better understanding of charge carrier dynamics in disordered conjugated polymers, and provide guidelines for the interpretation of measured THz mobility spectra.

ASSOCIATED CONTENT

Supporting Information

(1) Description of the procedure for fitting of the interring torsion terms in classical force field, (2) the comparison of CPM and DFT/LDA results, (3) the details of the application of the OFM and the verification of its accuracy, (4) the density of phonon states, (5) the comparison of transition rates obtained by two approaches, and (6) THz mobility spectra for different realizations of the system. This material is available free of charge via the Internet at http://pubs.acs.org.

AUTHOR INFORMATION

Corresponding Author

*E-mail: nenad.vukmirovic@ipb.ac.rs.

Notes

The authors declare no competing financial interest.

ACKNOWLEDGMENTS

N.V. is supported by European Community FP7 Marie Curie Career Integration Grant (ELECTROMAT), Serbian Ministry of Science (project ON171017), and FP7 projects PRACE-1IP, PRACE-2IP, HP-SEE, and EGI-InSPIRE. The Swedish Energy Agency (STEM), the Swedish Research Council, the Knut & Alice Wallenberg foundation and the European Research Council (Advanced Investigator Grant to V.S., 226136-VISCHEM) are also acknowledged.

REFERENCES

(1) Forrest, S. R. *Nature (London)* **2004**, *428*, 911−918.
(2) Berggren, M.; Nilsson, D.; Robinson, N. D. *Nat. Mater.* **2007**, *6*, 3−5.
(3) Kim, Y.; Cook, S.; Tuladhar, S. M.; Choulis, S. A.; Nelson, J.; Durrant, J. R.; Bradley, D. D. C.; Giles, M.; McCulloch, I.; Ha, C.-S.; Ree, M. *Nat. Mater.* **2006**, *5*, 197−203.
(4) Klauk, H.; Zschieschang, U.; Pflaum, J.; Halik, M. *Nature (London)* **2007**, *445*, 745−749.
(5) Yan, H.; Chen, Z.; Zheng, Y.; Newman, C.; Quinn, J. R.; Dötz, F.; Kastler, M.; Facchetti, A. *Nature (London)* **2009**, *457*, 679−686.
(6) Rogers, J. A.; Someya, T.; Huang, Y. *Science* **2010**, *327*, 1603−1607.
(7) Giri, G.; Verploegen, E.; Mannsfeld, S. C. B.; Atahan-Evrenk, S.; Kim, D. H.; Lee, S. Y.; Becerril, H. A.; Aspuru-Guzik, A.; Toney, M. F.; Bao, Z. *Nature (London)* **2011**, *480*, 504−508.
(8) Coropceanu, V.; Cornil, J.; da Silva Filho, D. A.; Olivier, Y.; Silbey, R.; Bredas, J.-L. *Chem. Rev.* **2007**, *107*, 926−952.
(9) Tiwari, S.; Greenham, N. C. *Opt. Quantum. Electron.* **2009**, *41*, 69−89.
(10) Tanase, C.; Meijer, E. J.; Blom, P. W. M.; de Leeuw, D. M. *Phys. Rev. Lett.* **2003**, *91*, 216601.
(11) Craciun, N. I.; Wildeman, J.; Blom, P. W. M. *Phys. Rev. Lett.* **2008**, *100*, 056601.
(12) Vukmirović, N.; Wang, L.-W. *Nano Lett.* **2009**, *9*, 3996−4000.
(13) Bredas, J. L.; Norton, J. E.; Cornil, J.; Coropceanu, V. *Acc. Chem. Res.* **2009**, *42*, 1691−1699.

(14) Ulbricht, R.; Hendry, E.; Shan, J.; Heinz, T. F.; Bonn, M. *Rev. Mod. Phys.* **2011**, *83*, 543−586.
(15) Němec, H.; Kužel, P.; Sundström, V. *J. Photochem. Photobiol., A* **2010**, *215*, 123−139.
(16) Kitamura, C.; Tanaka, S.; Yamashita, Y. *Chem. Mater.* **1996**, *8*, 570−578.
(17) Inganäs, O.; Zhang, F.; Andersson, M. R. *Acc. Chem. Res.* **2009**, *42*, 1731−1739.
(18) Inganäs, O.; Svensson, M.; Zhang, F.; Gadisa, A.; Persson, N. K.; Wang, X.; Andersson, M. R. *Appl. Phys. A: Mater. Sci. Process.* **2004**, *79*, 31−35.
(19) Pal, S. K.; Kesti, T.; Maiti, M.; Zhang, F.; Inganäs, O.; Hellström, S.; Andersson, M. R.; Oswald, F.; Langa, F.; Österman, T.; Pascher, T.; Yartsev, A.; Sundström, V. *J. Am. Chem. Soc.* **2010**, *132*, 12440−12451.
(20) Němec, H.; Nienhuys, H.-K.; Zhang, F.; Inganäs, O.; Yartsev, A.; Sundström, V. *J. Phys. Chem. C* **2008**, *112*, 6558−6563.
(21) Ponseca, C. S., Jr.; Němec, H.; Vukmirović, N.; Fusco, S.; Wang, E.; Andersson, M.; Chabera, P.; Yartsev, A.; Sundström, V. *J. Phys. Chem. Lett.* **2012**, *3*, 2442−2446.
(22) Yang, H.-C.; Hua, C.-Y.; Kuo, M.-Y.; Huang, Q.; Chen, C.-L. *ChemPhysChem* **2004**, *5*, 373−381.
(23) Kilina, S.; Batista, E.; Yang, P.; Tretiak, S.; Saxena, A.; Martin, R. L.; Smith, D. *ACS Nano* **2008**, *2*, 1381−1388.
(24) Yang, P.; Batista, E. R.; Tretiak, S.; Saxena, A.; Martin, R. L.; Smith, D. L. *Phys. Rev. B* **2007**, *76*, 241201.
(25) McMahon, D. P.; Troisi, A. *Chem. Phys. Lett.* **2009**, *480*, 210−214.
(26) Ruhle, V.; Kirkpatrick, J.; Andrienko, D. *J. Chem. Phys.* **2010**, *132*, 134103.
(27) Cheung, D. L.; McMahon, D. P.; Troisi, A. *J. Am. Chem. Soc.* **2009**, *131*, 11179−11186.
(28) Vukmirović, N.; Wang, L.-W. *J. Phys. Chem. B* **2009**, *113*, 409−415.
(29) Zhang, G.; Pei, Y.; Ma, J.; Yin, K.; Chen, C.-L. *J. Phys. Chem. B* **2004**, *108*, 6988−6995.
(30) Zhang, G.; Ma, J.; Wen, J. *J. Phys. Chem. B* **2007**, *111*, 11670−11679.
(31) Vukmirović, N.; Wang, L.-W. *Phys. Rev. B* **2010**, *81*, 035210.
(32) Zhang, X.; Li, Z.; Lu, G. *Phys. Rev. B* **2010**, *82*, 205210.
(33) Vukmirović, N.; Wang, L.-W. *J. Phys. Chem. B* **2011**, *115*, 1792−1797.
(34) Granadino-Roldan, J.; Vukmirović, N.; Fernandez-Gomez, M.; Wang, L.-W. *Phys. Chem. Chem. Phys.* **2011**, *13*, 14500−14509.
(35) Anselmo, A. S.; Lindgren, L.; Rysz, J.; Bernasik, A.; Budkowski, A.; Andersson, M. R.; Svensson, K.; van Stam, J.; Moons, E. *Chem. Mater.* **2011**, *23*, 2295−2302.
(36) Hwang, M. J.; Stockfisch, T. P.; Hagler, A. T. *J. Am. Chem. Soc.* **1994**, *116*, 2515−2525.
(37) Maple, J. R.; Hwang, M.-J.; Stockfisch, T. P.; Dinur, U.; Waldman, M.; Ewig, C. S.; Hagler, A. T. *J. Comput. Chem.* **1994**, *15*, 162−182.
(38) Becke, A. D. *J. Chem. Phys.* **1993**, *98*, 5648.
(39) Stephens, P. J.; Devlin, F. J.; Chabalowski, C. F.; Frisch, M. J. *J. Phys. Chem.* **1994**, *98*, 11623−11627.
(40) *LAMMPS Molecular Dynamics Simulator;* http://lammps.sandia.gov (accessed September 3, 2012).
(41) Plimpton, S. J. *J. Comput. Phys.* **1995**, *117*, 1−19.
(42) Bylaska, E. J.; et al. *NWChem, A Computational Chemistry Package for Parallel Computers*, version 5.1; Pacific Northwest National Laboratory: Richland, WA, 2007.
(43) Vukmirović, N.; Wang, L.-W. *J. Chem. Phys.* **2008**, *128*, 121102.
(44) Vukmirović, N.; Wang, L.-W. *J. Chem. Phys.* **2011**, *134*, 094119.
(45) Vukmirović, N.; Wang, L.-W. *Appl. Phys. Lett.* **2010**, *97*, 043305.
(46) Scher, H.; Lax, M. *Phys. Rev. B* **1973**, *7*, 4491−4502.
(47) Grozema, F. C.; Siebeless, L. D. A. *Int. Rev. Phys. Chem.* **2008**, *27*, 87−138.
(48) Němec, H.; Nienhuys, H.-K.; Perzon, E.; Zhang, F.; Inganäs, O.; Kužel, P.; Sundström, V. *Phys. Rev. B* **2009**, *79*, 245326.
(49) Bässler, H. *Phys. Status Solidi B* **1993**, *175*, 15−56.
(50) Movaghar, B.; Grünewald, M.; Ries, B.; Bassler, H.; Würtz, D. *Phys. Rev. B* **1986**, *33*, 5545−5554.
(51) Ponseca, C. S., Jr.; Yartsev, A.; Wang, E.; Andersson, M. R.; Vithanage, D.; Sundström, V. *J. Am. Chem. Soc.* **2012**, *134*, 11836−11839.

Supporting information for: Insights into the charge carrier terahertz mobility in polyfluorenes from large-scale atomistic simulations and time-resolved terahertz spectroscopy

Nenad Vukmirović,[*,†] Carlito S. Ponseca Jr.,[‡] Hynek Němec,[¶] Arkady Yartsev,[‡] and Villy Sundström[‡]

Scientific Computing Laboratory, Institute of Physics Belgrade, University of Belgrade, Pregrevica 118, 11080 Belgrade, Serbia, Division of Chemical Physics, Lund University, Box 124, 221 00 Lund, Sweden, and Institute of Physics, Academy of Sciences of the Czech Republic, 182 21 Prague, Czech Republic

E-mail: nenad.vukmirovic@ipb.ac.rs

[*]To whom correspondence should be addressed

[†]Scientific Computing Laboratory, Institute of Physics Belgrade, University of Belgrade, Pregrevica 118, 11080 Belgrade, Serbia

[‡]Division of Chemical Physics, Lund University, Box 124, 221 00 Lund, Sweden

[¶]Institute of Physics, Academy of Sciences of the Czech Republic, 182 21 Prague, Czech Republic

Fitting of the interring torsion terms in the classical force field

A deficiency of many general classical force fields (including the CFF91) is their inability to properly describe the interring torsion potentials. The most important torsion angles that actually determine the shape of the polymer chains are the angles S456 and 123S denoted in Figure 1. Therefore, we have modified the interring torsion potential terms to reproduce the ones obtained from quantum chemical calculations according to the following procedure.

First, a quantum chemical calculation of the total energy of the monomer structure shown in Figure 1 was performed for different values of the torsion angle S456, while all other internal coordinates of the molecule were kept fixed. The quantum chemical calculation was based on density functional theory (DFT) with the hybrid B3LYP functional[1,2] and the 6-31G basis set. From this calculation one obtains the quantum chemical torsion potential profile $E_1(\alpha)$, shown in dots in Figure 2, where α is the torsion angle. Next, the dependence of the energy of the structure on the same torsion angle $E_1'(\alpha)$ was calculated using a classical force field, where all interring torsion potentials were removed from the force field. The difference $E_1(\alpha) - E_1'(\alpha)$ was then fitted to an expression $f_1(t) = a_0 + a_1 \cdot t + a_2 \cdot t^2 + a_3 \cdot t^3 + a_4 \cdot t^4$, where $t = \cos\alpha$. The best fit was obtained with the parameters $a_0 = 9.1371\,\frac{\text{kcal}}{\text{mol}}$, $a_1 = -0.0092351\,\frac{\text{kcal}}{\text{mol}}$, $a_2 = -6.7663\,\frac{\text{kcal}}{\text{mol}}$, $a_3 = 1.5724\,\frac{\text{kcal}}{\text{mol}}$, $a_4 = -0.68487\,\frac{\text{kcal}}{\text{mol}}$.

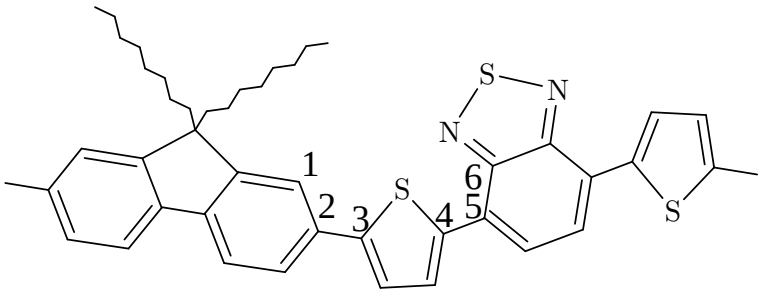

Figure 1: Chemical structure of APFO-3 polymer. The relevant interring torsion angles 123S and S456 are denoted in the figure.

Next, the same procedure was repeated where the angle 123S was changed, rather than S456. The difference between quantum chemical energy $E_2(\alpha)$ (shown in dots in Figure 3) and classical force field without the interring potentials energy $E_2'(\alpha)$ was again fitted to the expression $f_2(t) =$

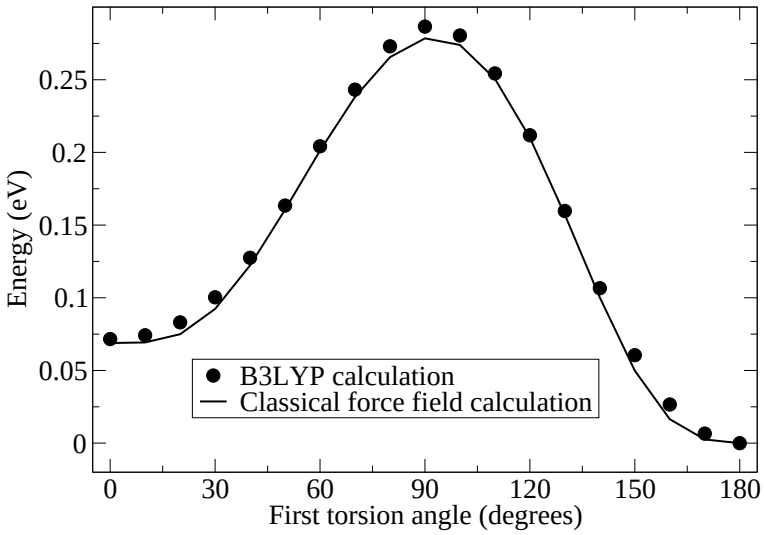

Figure 2: The dependence of the energy of the structure on the first torsion angle (the angle denoted as S456 in Figure 1).

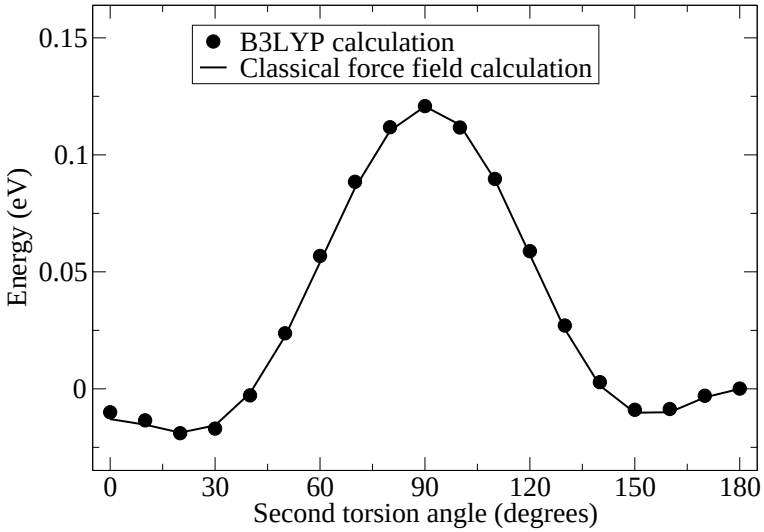

Figure 3: The dependence of the energy of the structure on the second torsion angle (the angle denoted as 123S in Figure 1).

$a_0 + a_1 \cdot t + a_2 \cdot t^2 + a_3 \cdot t^3 + a_4 \cdot t^4$ and the best fit was obtained with the parameters $a_0 = 4.5795 \frac{\text{kcal}}{\text{mol}}$, $a_1 = 0.59555 \frac{\text{kcal}}{\text{mol}}$, $a_2 = -7.0008 \frac{\text{kcal}}{\text{mol}}$, $a_3 = -0.65038 \frac{\text{kcal}}{\text{mol}}$, $a_4 = 2.4305 \frac{\text{kcal}}{\text{mol}}$.

Finally, to obtain the modified force field for use in this work, all interring torsion terms were removed and the terms $f_1(\alpha)$ and $f_2(\alpha)$ were added for each angle of the type S456 and 123S, respectively. Such a force field was then used in all molecular dynamics simulations performed in this work.

To verify that the modified force field reproduces well the interring torsion potentials, we have calculated the dependence of the energy of the structure on torsion angles S456 (solid line, Figure 2) and 123S (solid line, Figure 3). As seen, the modified force field reproduces well the results from a quantum chemical calculation.

Verification of the accuracy of the charge patching method

Since CPM is an approximation to a full DFT/LDA calculation, it is desirable to verify its accuracy on some smaller system where it is still feasible to perform a DFT/LDA calculation. Therefore, we have compared the results obtained by CPM and DFT/LDA for a 462 atom system (the system consists of 3 chains, each is 2 monomers long, with pentyl side chains). The comparison of the density of states obtained in these calculations is given in Figure 4. A good agreement between the results obtained by the two methods verifies that CPM provides the accuracy similar to that of DFT/LDA.

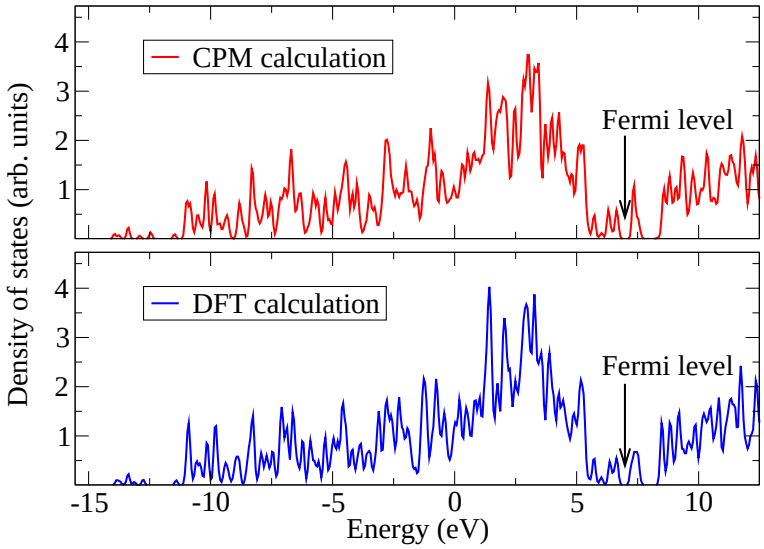

Figure 4: The comparison of the density of states of the 462 atom system calculated using the direct DFT/LDA calculation and the CPM.

The details of the application of the overlapping fragments method and the verification of its accuracy

The OFM is the method for the diagonalization of a single particle Hamiltonian – for example the one obtained using the CPM. It is based on the the division of the system into (mutually overlapping) fragments and the representation of the Hamiltonian in the basis of eigenfunctions of these fragments. The accuracy of the methodology crucially depends on the proper choice of fragments and the number of orbitals per fragment. The scheme for the division of the system into fragments in the OFM is shown in Figure 5. The basis consisting of one HOMO orbital per each fragment was used in the OFM.

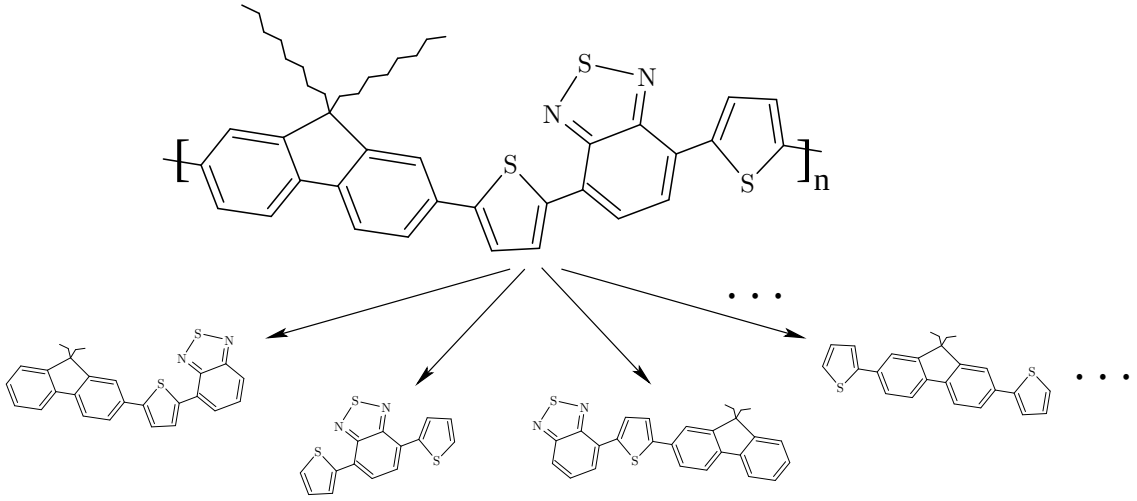

Figure 5: The scheme for the division of the system into fragments in the OFM. The basis consisting of one HOMO orbital per each fragment was used.

Since OFM is an approximation to the exact numerical diagonalization of the Hamiltonian, one has to verify its accuracy by comparing to the results of the diagonalization in the plane wave representation, which can be considered to give numerically exact values. The comparison was performed for a 2360 atom system (5 chains, each 5 monomers long, with octyl side chains) where plane wave diagonalization is still feasible. The results of the comparison, given in Figure 6, show that the OFM provides satisfactorily accurate eigenenergies.

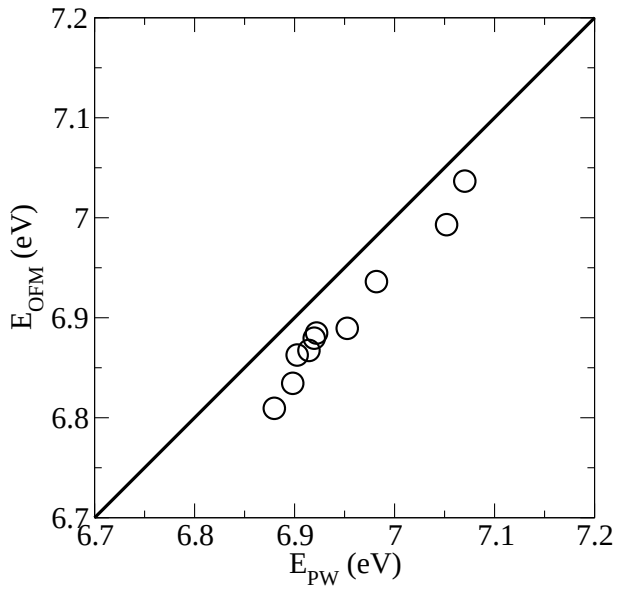

Figure 6: The comparison of eigenenergies obtained by diagonalization in the plane wave basis (E_{PW}) and the ones obtained by the OFM (E_{OFM})

The density of phonon states

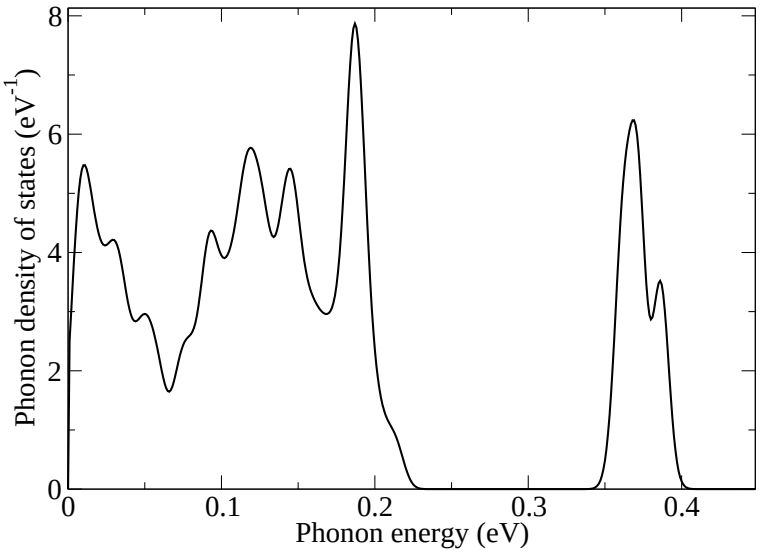

Figure 7: The density of phonon states of APFO-3 polymer.

The density of phonon states of the APFO-3 polymer was calculated from the same classical force field used in MD simulations and is shown in Figure 7.

The comparison of transition rates obtained by two methods

The comparison between W_{ij} and W_{ij}^{model} for various transitions in the 2360 atom system is shown in Figure 8. We note that the largest discrepancy between W_{ij} and W_{ij}^{model} is by a factor of 30, while for 90% of the points the discrepancy is smaller than by a factor of 10. The average discrepancy defined as $10^{\left\langle \left| \log_{10}\left(W_{ij}/W_{ij}^{\mathrm{model}}\right)\right| \right\rangle}$ (where $\langle \ldots \rangle$ denotes the average value) is equal to a factor of 3.8.

In our previous work[3] we have tested the applicability of the approximate expression for transition rates W_{ij}^{model} in comparison to W_{ij} in the case of P3HT polymer. A similar degree of discrepancy between W_{ij} and W_{ij}^{model} was obtained there (left panel of Figure 4 in that paper). Nevertheless, the temperature and electric field dependencies of the mobilities obtained using these two different models for transition rates were nearly identical (within few per cent, see Figures 3a and 3b in that paper). These results indicated that the transport properties are not very sensitive to the details of the individual transitions and that the approximation used is an excellent approximation if one wishes to model transport properties, as we do here.

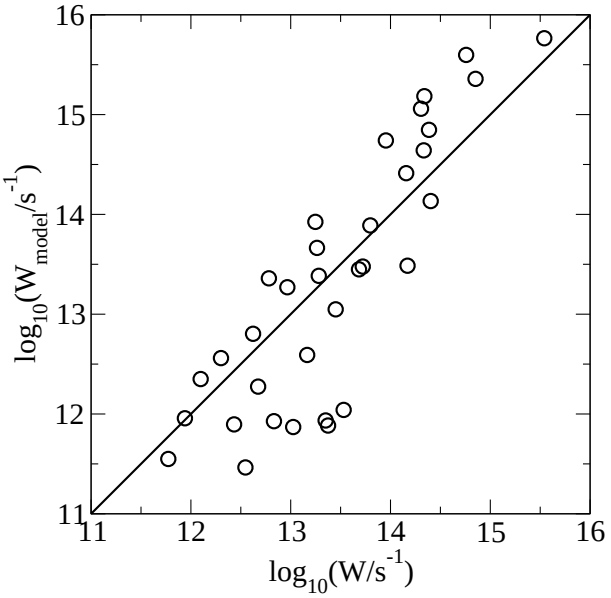

Figure 8: The comparison of transition rates W calculated by taking into account the interaction with all phonon modes and the transition rates W_{model} calculated using the model that considers only the wavefunction moduli overlap.

Frequency dependent mobility for different realizations of the system

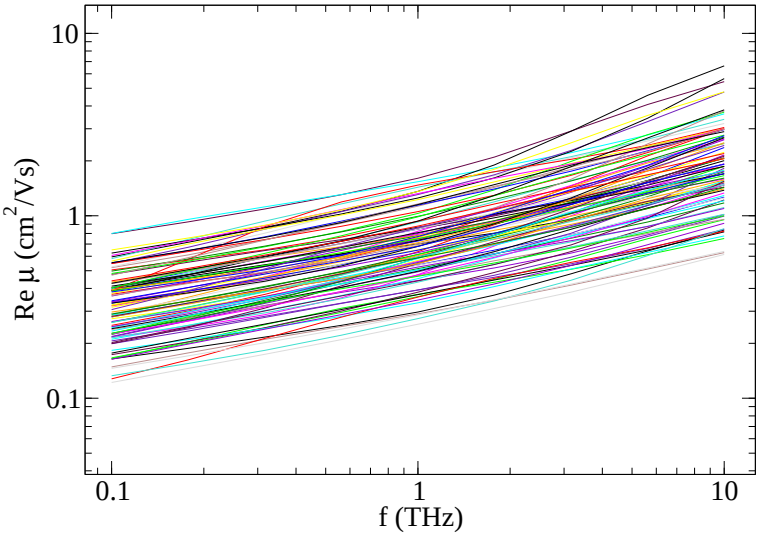

Figure 9: Frequency dependence of the real part of the mobility at a temperature of 300 K for 100 different realizations of the $4\times4\times4$ system.

References

(1) Becke, A. D. *J. Chem. Phys.* **1993**, *98*, 5648.

(2) Stephens, P. J.; Devlin, F. J.; Chabalowski, C. F.; Frisch, M. J. *J. Phys. Chem.* **1994**, *98*, 11623–11627.

(3) Vukmirović, N.; Wang, L.-W. *Appl. Phys. Lett.* **2010**, *97*, 043305.